A Mechanistic Study on the Photoisomerizations of Spiro[2,4]hept-1-ene, Vinylidenecyclopentane, and Vinylidenecyclobutane Hydrocarbons

Ming-Der Su*

Department of Applied Chemistry, National Chiayi University, Chiayi 60004, Taiwan

Received: November 19, 2007; Revised Manuscript Received: March 24, 2008

The mechanisms of photochemical isomerization reactions were investigated theoretically using the following model systems: spiro[2,4]hept-1-ene, 1-vinylcyclopentene, and vinylidenecyclobutane with the CASSCF/6-311G(d) (six-electron/six-orbital active space) and the MP2-CAS/6-311G(d,p)/CASSCF/6-311G(d) methods. The structures of the conical intersections, which play a central role in such photorearrangements, were obtained. The intermediates and transition structures of the ground states were also calculated to assist in providing a qualitative explanation of the reaction pathways. Our model investigations strongly indicate that a vinylcarbene-like intermediate can serve as a basis for discussion and rationalization of the results of the above photoisomerizations. Besides this, our theoretical findings suggest that the conical intersection mechanism found in this work gives a good explanation and supports the experimental observations. Also, all the relative final product yields predicted in the present work are in good agreement with the available experimental findings.

I. Introduction

Despite prolonged interest in the photoreactions of cyclopropenes,[1] bicyclic alkylcyclopropenes, their related allenes, have received surprisingly little attention.[2] The reason for this is probably because the parent chromophore is devoid of absorption above 210 nm and hence requires the use of far-UV techniques for its investigation. A recent report concerning the photochemistry of one bicyclic alkylcyclopropene derivative[3] has demonstrated that the photochemical behavior of alkylated systems differs in several respects from that of typical arylcyclopropenes[4] (see eq 1 in Scheme 1). That is, photolysis of spiro[2,4]hept-1-ene (**1**) in pentane solution with a low-pressure mercury lamp results in a rearrangement to the isomeric allene (vinylidenecyclopentene) **2**, alkyne (ethynylcyclopentane) **3**, and diene (1-vinylcyclopentene) **4** with quantum yields of 43%, 38%, and 13%, respectively.[2,3] Likewise, this can be compared to the results of thermolysis of **1** at 225 °C, which yields the alkyne **3** in 75% yield along with minor amounts of **4**.[2] On the other hand, photolysis (185 nm) of the five-membered exocyclic allene (vinylidenecyclopentane, **2**) yields the product distribution (**1**, **3**, **4**, and **5**)[2] as shown in eq 2 in Scheme 1. Direct photolysis of vinylidenecyclobutane (**6**) in deoxygenated solution at 185 nm produces spiro[2,3]hex-1-ene (**7**), ethynylcyclobutane (**8**), 3-methylenecyclopentene (**9**), ethylene (**10**), and photoproduct (**11**) in measurable yields.[5]

It is these fascinating experimental results that inspired this study. The key questions are how the various products are formed and why certain products show a significant abundance.[3–5] A knowledge of the features of the potential energy hypersurfaces is in general of great value in understanding the roles of the various possible processes. Although these experimental results help in understanding the potential energy surfaces of excited states in bicyclic alkylcyclopropene systems, they are at present not capable of providing complete mechanistic detail. We were thus curious about exactly how these reactions occur, and we wanted detailed mechanistic knowledge in order to exercise greater control over them. Nevertheless, it is very difficult to detect thermally unstable intermediates and transition structures of ground and excited states because of their short lifetimes. Theory is therefore a potentially useful partner to investigate the mechanism of such photoisomerizations. Besides, as far as we are aware, until now no quantum chemical studies have been performed on bicyclic alkylcyclopropene photorearrangements. It is astonishing how little is known about the mechanisms of photoisomerizations of bicyclic alkylcyclopropenes and their related allenes, considering the importance of cyclopropenes in synthetic as well as photochemistry.[1,6] We have thus undertaken the investigation of the potential energy surfaces of bicyclic alkylcyclopropene systems.

SCHEME 1

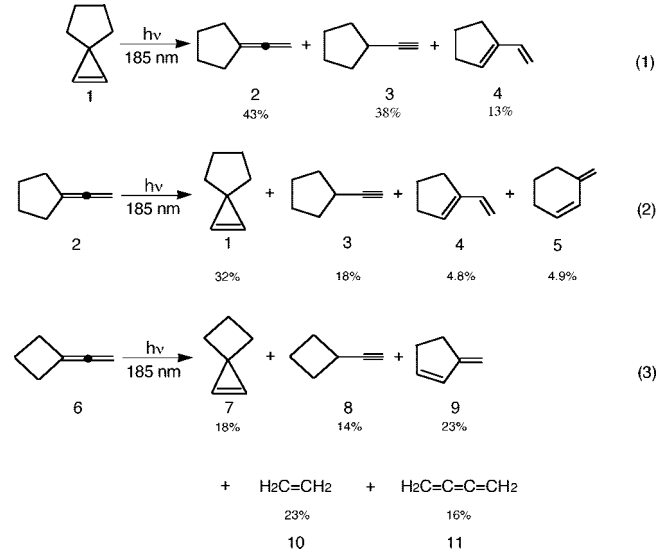

The object of this work is to gain an understanding of the photochemical mechanism of the transformation of bicyclic alkylcyclopropenes and their related allenes to various photoproducts. As illustrated in Scheme 1, the reaction mechanisms of three different reactions were investigated by CASSCF and

* To whom correspondence should be addressed: e-mail midesu@mail.ncyu.edu.tw.

10.1021/jp711022n CCC: $40.75
Published on Web 05/27/2008

MP2-CAS calculations: namely, spiro[2,4]hept-1-ene (**1**), vinylidenecyclopentane (**2**), and vinylidenecyclobutane (**6**) were used as model systems. It will be shown below that the conical intersections (CIs),[7] whose geometrical structure is vinylcarbene-like, play a crucial role in the photoisomerization of these bicyclic alkylcyclopropenes systems.

II. Methodology

All geometries were fully optimized without imposing any symmetry constraints, although in some instances the resulting structures showed various elements of symmetry. Ab initio molecular orbital calculations were performed with the Gaussian 03 software package.[8]

In the investigation of photochemical reaction pathways, the stationary point structures on S_0 and S_1 surfaces were optimized at the CASSCF (complete active space self-consistent field) level of calculations by use of the standard 6-311G(d) basis set.[9] The active space for describing the photoisomerizations of **1**, **2**, and **6** comprises six electrons in six orbitals—two p-π orbitals, plus two σ(C−C) and two σ*(C−C) orbitals—and is referred to as CASSCF(6,6). In some hydrogen shift molecules, their active space is chosen as two p-π orbitals, plus two σ (i.e., C−C and C−H) and two σ* (i.e., C−C and C−H) orbitals. The state-averaged CASSCF(6,6) method was used to determine geometry on the intersection space. The optimization of conical intersections was achieved in the (f - 2)-dimensional intersection space via the method of Bearpark et al.[10] implemented in the Gaussian 03 program.

The harmonic vibrational frequencies of all stationary points computed analytically at the CASSCF level were computed analytically to characterize them as minima (all frequencies are real) or transition states (only one imaginary frequency). The optimization was determined when the maximum force and its root-mean-square (rms) were less than 0.000 45 and 0.000 05 hartree/bohr, respectively. Localization of the minima, transition states, and conical intersection minima was performed in Cartesian coordinates; therefore, the results are independent of any specific choice of internal variables.

Further, 14 of the reactions that we have investigated have been probed in some detail by determining the intrinsic reaction coordinate (IRC)[11] with the algorithm proposed by Gonzalez and Schlegel.[12]

To correct the energetics for dynamic electron correlation, we have used the multireference Møller−Plesset algorithm[13] as implemented in the program package Gaussian 03. Unless otherwise noted, the relative energies given in the text are those determined at the MP2-CAS-(6,6)/6-311G(d,p) level by use of the CAS(6,6)/6-311G(d) (hereafter designed MP2-CAS and CASSCF, respectively) geometry. All calculations were carried out on the IBM computers at the National Center for High-Performance Computing, with the Gaussian 03 program.[8]

III. General Considerations

Although the cyclopropene derivative photoisomerizations reported experimentally[1,2,5] show a wide variance in their reaction types, it is still possible to construct a certain consistency in these reactions, which at least serves as a basis for discussion. In this section, we describe possible excited-state reaction paths that lead to the conical intersections. It is well-known that the photochemistry of cyclopropene derivatives is dominated by initial ring opening to produce vinylcarbene intermediates.[1,2,4] Indeed, as already shown in eq 1 in Scheme 1, photolysis of spiro[2,4]hept-1-ene (**1**) can yield substantial amounts of allene and alkyne products in addition to the 1,3-dienes that are characteristic of vinylcarbene-like intermediates.[1] Similarly, in the case of eq 2 in Scheme 1, Leigh[2] proposed a mechanism involving a vinylcarbene-like intermediate to explain the formation of a variety of photoproducts due to the photolysis of **2**. Namely, he considered that products **1**, **3**, and **4** all arise from the vinylcarbene derived from [1,2]-H migration in the excited singlet state of **2**.[2] Also, it has been reported that allenes produce cyclopropenes in both ground and singlet excited states via vinylcarbene intermediates.[1,4] In fact, it was reported that photochemical cyclopropene ring opening is considered to involve the S_1 state with the formation of the planar vinyl diradical[1,2] (see Scheme 2). Besides this, it was noted that the lowest excited triplet state of cyclopropene is unreactive toward ring opening and generally undergoes dimerization.[2] We thus do not consider the excited triplet state for the cyclopropene derivative systems any further. From the above discussion, it is evident that vinylcarbene-like intermediates should play a decisive role in the photochemical mechanisms of cyclopropene derivatives. Nevertheless, attempts to trap such intermediates with methanol or alkene have been unsuccessful so far.[4]

In the following section, we shall use the above mechanisms for locating the "funnel" from the excited-state surface to the ground-state surface that corresponds to a conical intersection.

SCHEME 2

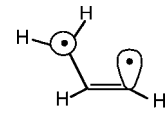

vinylmethylene

TABLE 1: Energies of Critical Points Located along Paths 1−6[a]

structure	state	ΔE_{rel}[b]
spiro[2,4]hept-1-ene (**1**)	S_0	0.0 (0.0)
FC-1	S_1	150.7 (172.1)
Int-2	S_1	101.7 (90.08)
TS-1	S_1	129.5 (118.8)
CI-1	S_1/S_0	60.72 (42.83)
Int-2	S_0	45.94 (25.36)
TS-2	S_0	51.06(49.83)
TS-3	S_0	65.74 (56.16)
CI-2	S_1/S_0	100.7 (144.1)
TS-4	S_0	79.56 (67.03)
TS-5	S_0	60.61 (64.53)
TS-6	S_0	28.44 (40.17)
2	S_0	−15.98(−30.84)
3	S_0	−60.86 (−30.02)
4	S_0	−3.426 (−38.07)

[a] Energies were calculated at the MP2-CAS(6,6)/6-311G(d,p)//CAS-(6,6)/6-311G(d) and CAS(6,6)/6-311G(d) (values in parentheses) levels of theory and are given in kilocalories per mole. See Figures 1–3 and Figure B in Supporting Information. [b] Energy relative to spiro[2,4]hept-1-ene (**1**).

IV. Results and Discussion

(1) Spiro[2,4]hept-1-ene (C_7H_{10}). We first consider the photochemical rearrangement reactions of spiro[2,4]hept-1-ene (**1**). As stated earlier, there could be three kinds of reaction pathways for the photoisomerization reactions of **1**, paths 1−3, which may lead to the final photoproducts vinylidenecyclopentene (**2**), alkyne (**3**), and 1,3-diene (**4**), respectively. Figure 1 displays the reaction profiles computed for eq 1 in Scheme 1 and contains the relative energies of the various points with respect to the

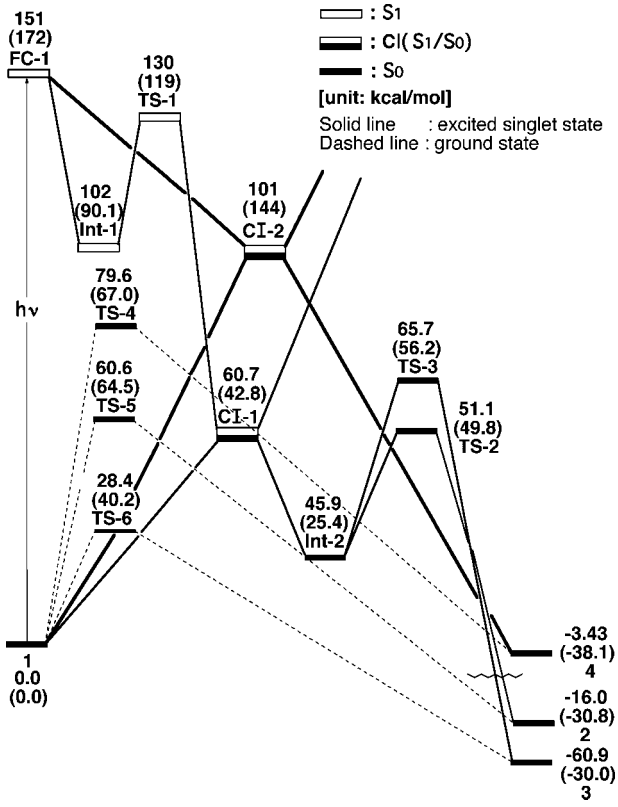

Figure 1. Energy profiles for the photoisomerization modes of spiro[2,4]hept-1-ene (**1**). FC, Franck−Condon; CI, conical intersection. Relative energies were obtained at the MP2-CAS-(6,6)/6-311G(d,p)//CAS(6,6)/6-311G(d) and CAS(6,6)/6-311G(d) (values in parentheses) levels of theory. All energies (in kilocalories per mole) are given with respect to the reactant (**1**). For CASSCF optimized structures of the crucial points, see Figures 2 and 3. For more information see the text.

energy of reactant **1**. Selected geometrical values and the relative energies based on CASSCF and MP2-CAS calculations for all the stationary points of **1** are reported in Figure 2 and Table 1, respectively. Cartesian coordinates are given in the Supporting Information.

The vertical excitation energy (**FC-1**) is calculated to lie 172 kcal/mol above the ground-state surface at the CAS(6,6)/6-311G(d) optimized reactant geometry **1**. This value drops to 151 kcal/mol after correction via MP2-CAS calculations, which is surprisingly close to the experimental absorption band (185 nm = 155 kcal/mol).[3] It is thus believed that the present model compound with the method employed in this study should provide reliable information for the discussion of the singlet photochemical reaction mechanisms of **1**.

Once $S_0 \rightarrow S_1$ vertical excitation occurs, the system will relax from the **FC-1** point [$S_1(S_0$ geom)] to the S_1 minimum **Int-2** [$S_1(S_1$ geom)], which is lower in energy than the former by 49 kcal/mol. The optimized geometrical parameters of **Int-1**can be found in Figure 2. Our CASSCF results indicate that the **Int-1** structure has two shorter C−C bond distances (1.447 and 1.454 Å) and a longer C−C bond length (1.834 Å) than its closed-shell singlet state. This strongly implies that one C−C bond of the triangular ring (**Int-1**) compound is broken during the photochemical isomerization of **1**.

After the local minimum **Int-1**, we found a transition state **TS-1**, which is based on the model of reactant **1**. The optimized transition-state structure (**TS-1**) along with the calculated transition vector at the CASSCF level is given in Figure 2. The arrows indicate the direction in which the three carbon atoms of the triangular ring vibrate in the normal coordinate corresponding to the imaginary frequency ($821i$ cm^{-1}). As seen in Figure 1 and Table 1, it is apparent that the transition structure (**TS-1**) for the ring opening process is lower in energy by 21 kcal/mol than the corresponding **FC-1**, but it is higher in energy by 18 kcal/mol than the local intermediate **Int-1**. Accordingly, owing to the large excess energy (49 kcal/mol) obtained from the decay of **FC-1** to **Int-1**, it is expected that this relaxation energy is sufficient to provoke the effective photoisomerization reactions (paths 1 and 2) for **1** (vide infra).

Furthermore, through the transition state **TS-1**, the lowest energy point of the intersection seam of the S_0 and S_1 state was located for the ring opening process. This was identified as **CI-1** as presented in Figures 1 and 2. As one can see in Figure 2, the structure of **CI-1** is quite vinylcarbene-like, just as we predicted in the previous section. Funneling through the S_0/S_1 **CI-1** conical intersection can lead to two different reaction pathways on the ground-state surface via either the derivative coupling vector or the gradient difference vector.[7] The gradient difference vector for **CI-1**corresponds to a CCC vibrating motion, which may lead to a vibrationally hot species at the S_0 configuration. On the other hand, its derivative coupling vector corresponds to a C−C bond stretching motion, which can result in another planar intermediate **Int-2**. It should be noted here that although the energy is minimized, the structure **CI-1** shown in Figures 1 and 2 is just a conical intersection rather than a true minimum,[7] because its energy gradient does not go to zero. Moreover the MP2-CAS computational results indicate that the energy of **CI-1** relative to the ground-state minimum (**1**) is 61 kcal/mol, but it is lower than that of **FC-1** by 90 kcal/mol. Also, the MP2-CAS results demonstrate that the energy of **Int-2** is 105 kcal/mol lower than that of **FC-1** but higher than that of reactant **1**by 46 kcal/mol.

Again, after the local minimum **Int-2** on the S_0 potential energy surface is produced, there could be two reaction pathways (**TS-2** and **TS-3**), from which one may obtain the final photoproducts **2** and **3**, respectively. From Figure 1 and Table 1, it is clear that the transition state **TS-2** for intermediate **Int-2**, leading to product **2**, lies below the energy of **TS-3**, which connects the intermediate **Int-2** and product **3**, by 15 kcal/mol. We have done the IRC calculations to confirm this (for instance, see Figure A in Supporting Information). In consequence, our theoretical findings indicate that path 1 should be more favorable than path 2 from an energetic viewpoint. Therefore the product of path 1 (**2**; allene) is predicted to be produced in a larger quantum yield than that of path 2 (**3**; alkyne). The supporting evidence comes from the fact that, as already mentioned in eq 1 in Scheme 1, one major product (**2**) and two minor products (**3** and **4**) were observed in the photoisomerization reaction of spiro[2,4]hept-1-ene (**1**).[3] Consequently, our theoretical investigations suggest that the reaction mechanisms for paths 1 and 2 should proceed as follows:

Path 1: $\mathbf{1}\,(S_0) + h\nu \rightarrow$

$$\mathbf{FC\text{-}1} \rightarrow \mathbf{Int\text{-}1} \rightarrow \mathbf{TS\text{-}1} \rightarrow \mathbf{CI\text{-}1} \rightarrow \mathbf{Int\text{-}2} \rightarrow \mathbf{TS\text{-}2} \rightarrow \mathbf{2}$$

Path 2: $\mathbf{1}\,(S_0) + h\nu \rightarrow$

$$\mathbf{FC\text{-}1} \rightarrow \mathbf{Int\text{-}1} \rightarrow \mathbf{TS\text{-}1} \rightarrow \mathbf{CI\text{-}1} \rightarrow \mathbf{Int\text{-}2} \rightarrow \mathbf{TS\text{-}3} \rightarrow \mathbf{3}$$

We have also explored the mechanism of path 3, which contains only a single conical intersection point (S_1/S_0 **CI-2**). The derivative coupling and gradient difference vectors obtained at the conical intersection are given in Figure 3. Our MP2-CAS results suggest that S_1/S_0 **CI-2** is lower in energy than **FC-1** by

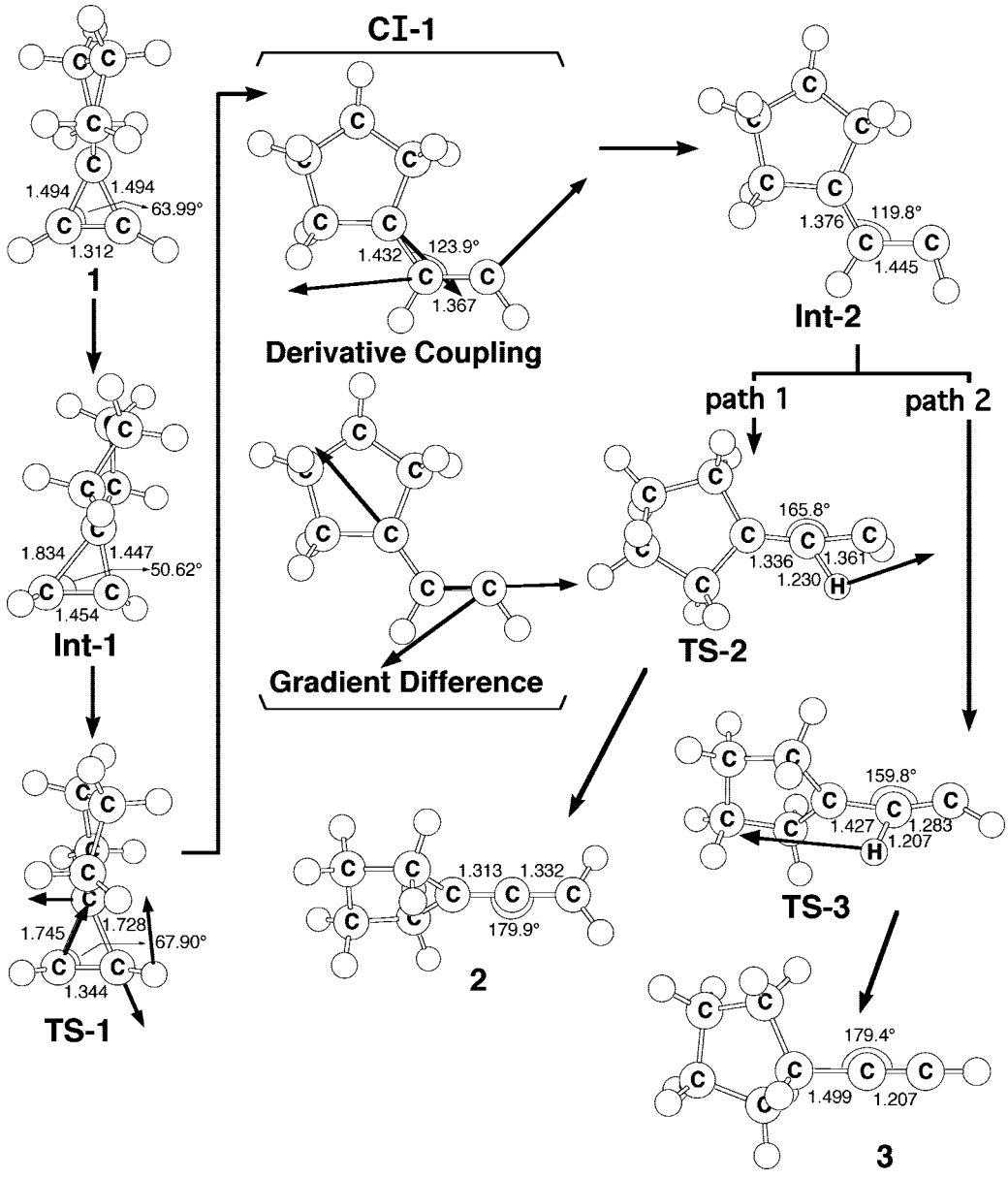

Figure 2. CAS(6,6)/6-311G(d) geometries (bond lengths in angstroms, angles in degrees) for paths 1 and 2 of spiro[2,4]hept-1-ene (**1**), conical intersection (**CI**), intermediates (**Int**), transition states (**TS**), and isomer products. Derivative coupling and gradient difference vectors—those that lift the degeneracy—were computed with CASSCF at **CI-1**. Corresponding CASSCF vectors are shown as insets. Heavy arrows indicate the main atomic motions in the transition-state eigenvector. For more information see Supporting Information.

40 kcal/mol but higher in energy than the corresponding reactant **1** by 101 kcal/mol. The existence of a low-lying conical intersection provides a highly effective radiationless decay channel.[7] Beside this, our computations predict that the photochemical rearrangement reaction of path 3 should be a barrierless process. That is, starting from the **FC-1** point, spiro[2,4]hept-1-ene (**1**) enters an extremely efficient decay channel, S_1/S_0 **CI-2**. After decay at this conical intersection point, the photoisomer **4** as well as the initial reactant **1** can be reached via a barrierless ground-state relaxation pathway. Accordingly, this work suggests that the reaction mechanism for path 3 should be as follows:

$$\text{Path 3:}\quad \mathbf{1}\,(S_0) + h\nu \rightarrow \mathbf{FC\text{-}1} \rightarrow \mathbf{CI\text{-}2} \rightarrow \mathbf{4}$$

In addition, as shown in Figure 1, our computational results indicate that the two conical intersection points (**CI-1** and **CI-2**) are 90 and 40 kcal/mol lower in energy than **FC-1**, respectively. Competition between these reaction paths is presumably governed by the surface shape and dynamical factors. As illustrated in Figure 1, the energy difference between these two conical intersections is substantial (about 40 kcal/mol). Paths 1−3 compete with each other, paths 1 and 2 being energetically more feasible from a kinetic viewpoint. The quantum yield of **2** and **3**are therefore expected to be larger than that of **4**. The energetic arguments are in qualitative agreement with the experimentally observed relative product distributions of **2**, **3**, and **4**, as already shown in eq 1 in Scheme 1.[3]

Furthermore, we have also investigated the ground-state (thermal) potential surfaces of **1**, which are given in Figure 1 and Figure B in Supporting Information. The search for transition states on the S_0 surface near the structures of S_1/S_0 **CI-1** gives **TS-4**, **TS-5**, and **TS-6**, which connect **1** and **4**, **1** and **2**, and **1** and **3**, respectively. Our model calculations demonstrate that these transition states all involve hydrogen migration with the calculated imaginary frequencies 138*i*, 1031*i*, and 1062*i* cm^{-1}, respectively. In consequence, our theoretical

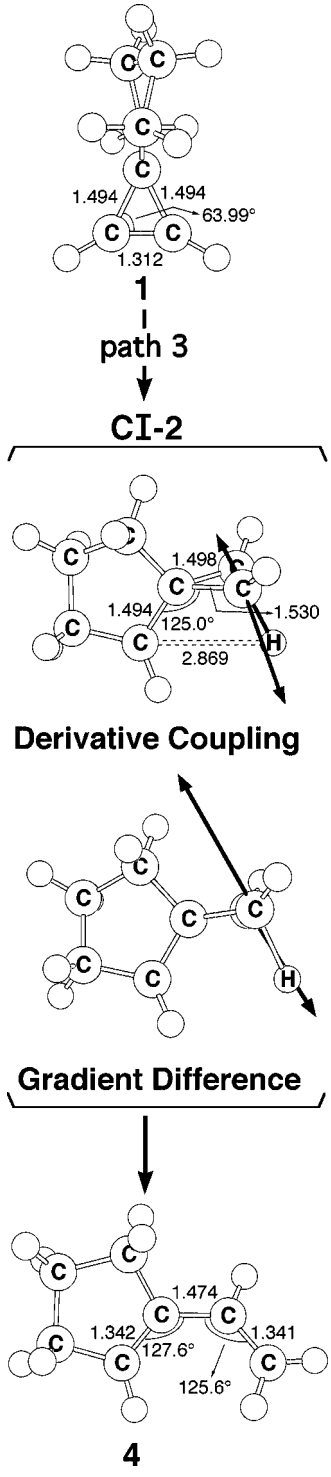

Figure 3. CAS(6,6)/6-311G(d) geometries (bond lengths in angstroms, angles in degrees) for path 3 of spiro[2,4]hept-1-ene (**1**), conical intersection (**CI**), and isomer product **4**. Derivative coupling and gradient difference vectors—those that lift the degeneracy—were computed with CASSCF at **CI-2**. Corresponding CASSCF vectors are shown as insets. For more information see Supporting Information.

investigations suggest that the reaction mechanisms for paths 8−10 should proceed as follows:

Path 4: **1** → **TS-4** → **4**

Path 5: **1** → **TS-5** → **2**

Path 6: **1** → **TS-6** → **3**

The barrier heights for these three reaction pathways are computed to be 80, 61, and 28 kcal/mol, respectively. This strongly implies that in the thermal reactions the yield of product alkyne (**3**) should be greater than that of either **2** or **4**. Again, our theoretical findings are in good agreement with the available experimental work.[3]

In short, our model investigations provide a qualitative explanation of the photoisomerization of **1** to final photoproducts via conical intersections as well as via thermal reactions. That is, an efficient photoisomerization occurs when the photoexcited reactant **1*** evolves along barrierless excited-state paths, decays

TABLE 2: Energies of Critical Points Located along Paths 7−10[a]

structure	state	ΔE_{rel}[b]
vinylidenecyclopentene (**2**)	S_0	0.0 (0.0)
FC-2	S_1	152.2 (152.0)
CI-3	S_1/S_0	93.71 (77.29)
Int-3	S_0	75.85 (58.55)
TS-7	S_0	82.88 (65.42)
TS-8	S_0	90.22 (78.29)
TS-9	S_0	97.09 (84.46)
CI-4	S_1/S_0	102.5 (58.55)
Int-4	S_0	30.04 (51.06)
TS-10	S_0	87.51 (90.60)
Int-5	S_0	73.43 (70.86)
TS-11	S_0	76.35 (52.59)
1	S_0	60.86 (30.02)
3	S_0	44.88 (−0.8158)
4	S_0	57.44 (−8.051)
5	S_0	32.96 (−14.46)

[a] Energies were calculated at the MP2-CAS(6,6)/6-311G(d,p)//CAS-(6,6)/6-311G(d) and CAS(6,6)/6-311G(d) (values in parentheses) levels of theory and are given in kilocalories per mole. See Figures 4 and 5 and Figures C and D in Supporting Information. [b] Energy relative to vinylidenecyclopentene (**2**).

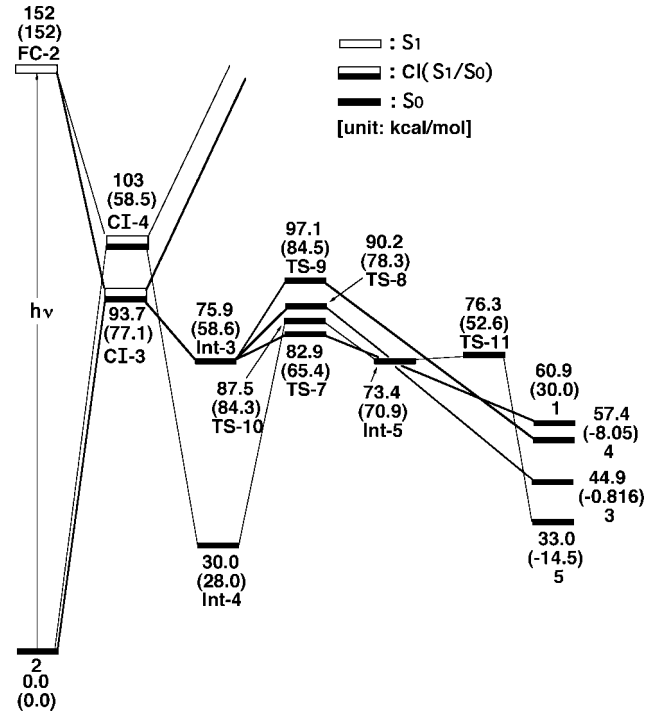

Figure 4. Energy profiles for the photoisomerization modes of vinylidenecyclopentene (**2**). FC, Franck−Condon; CI, conical intersection. Relative energies were obtained at the MP2-CAS-(6,6)/6-311G(d,p)//CAS(6,6)/6-311G(d) and CAS(6,6)/6-311G(d) (values in parentheses) levels of theory. All energies (in kilocalories per mole) are given with respect to the reactant (**2**). For CASSCF optimized structures of the crucial points, see Figure 5 and Figures C and D in Supporting Information. For more information see the text.

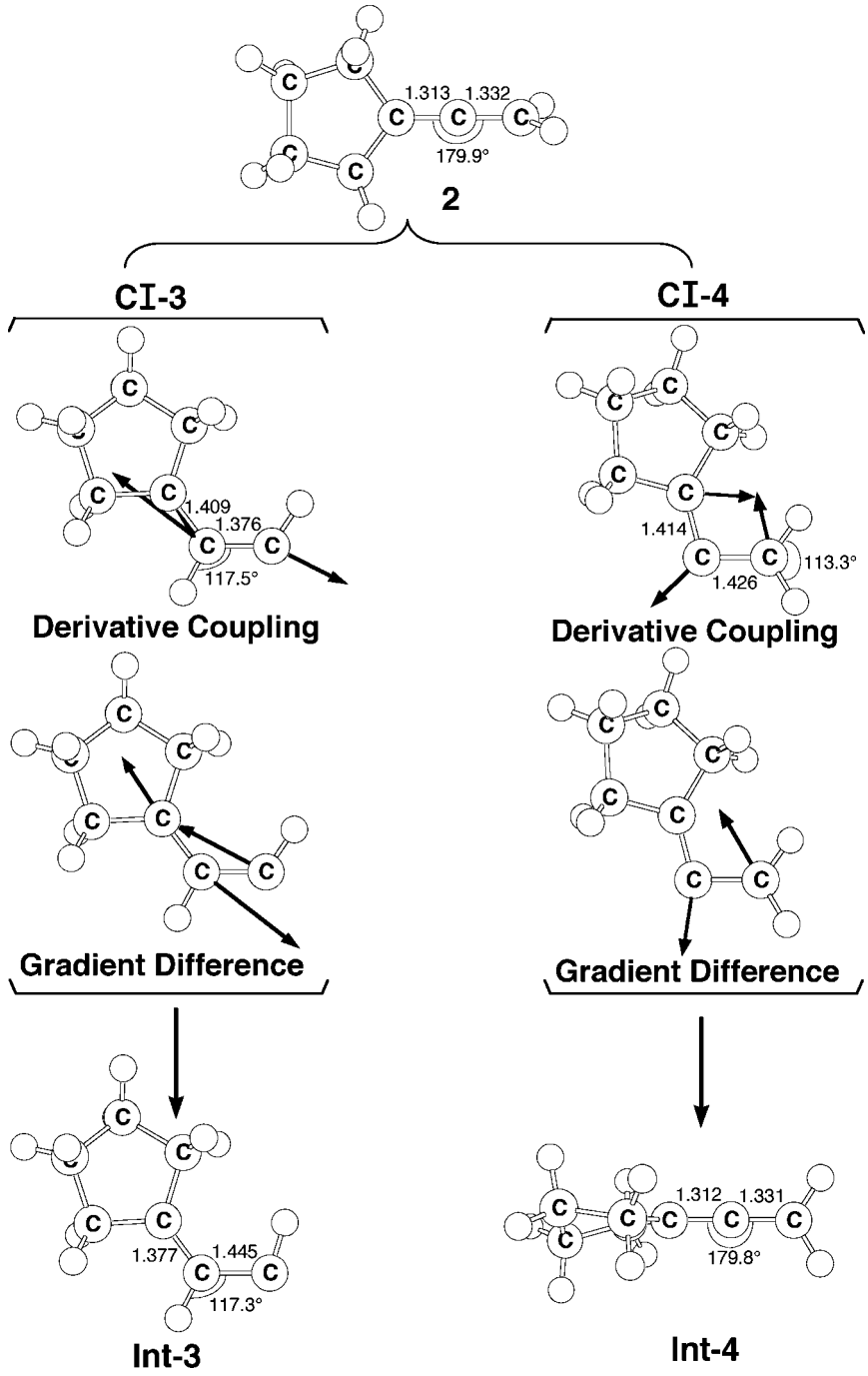

Figure 5. CAS(6,6)/6-311G(d,p) geometries (bond lengths in angstroms, angles in degrees) for paths 7−10 of vinylidenecyclopentene (**2**), conical intersections (**CI**), and intermediates (**Int**). Derivative coupling and gradient difference vectors—those that lift the degeneracy—were computed with CASSCF at **CI-3** and **CI-4**. Corresponding CASSCF vectors are shown as insets. Heavy arrows indicate the main atomic motions in the transition-state eigenvector. For more information see Supporting Information.

at conical intersection points, and after several chemical steps finally relaxes to the ground state between **1** and photoproducts (**2**, **3**, and **4**). The present calculations also indicate that the energy of the conical intersection **CI-1** for paths 1 and 2 is lower than that of the other conical intersection (**CI-2**). In consequence, path 1 should be the most favorable pathway in the photorearrangement reactions of spiro[2,4]hept-1-ene (**1**). Our theoretical conclusions agree well with the relative quantum yields of various photoproducts based on the experimental observations.[3] On the other hand, our theoretical work also demonstrates that path 6 should be the preferred route in the thermal reactions of **1**, giving **3** as the major product. Again, these theoretical findings are in accordance with the experimental observations.[2,3]

(2) Vinylidenecyclopentane (2). For comparison, we next consider the photoisomerizations (eq 2 in Scheme 1) of vinylidenecyclopentane **2**. In this section we shall again examine the photochemical reaction pathways corresponding to a vinylcarbene mechanism as described in the previous section. The discussion of these reaction pathways will be based on 14 fully optimized structures corresponding to minima, transition states, and real crossing points on the S_0 and S_1 ($\pi\pi^*$) potential surfaces. A schematic overview of the computed energy profiles for the photoreaction pathways of **2** is shown in Figure 4. The structures optimized at the CASSCF/6-311G(d) level are outlined in Figure 5 and Figures C and D in Supporting Information, with the corresponding energies based on CASSCF

TABLE 3: Energies of Critical Points Located along Paths 11−14[a]

structure	state	ΔE_{rel}[b]
vinylidenecyclobutane (**6**)	S_0	0.0 (0.0)
FC-3	S_1	157.0 (144.1)
CI-5	S_1/S_0	91.43 (88.60)
Int-6	S_0	60.86(59.66)
TS-12	S_0	62.59 (64.66)
TS-13	S_0	79.80 (86.77)
CI-6	S_1/S_0	43.82 (79.15)
Int-7	S_0	34.13 (10.66)
TS-14	S_0	67.75 (74.21)
Int-8	S_0	35.41(31.09)
TS-15	S_0	47.16 (47.32)
7	S_0	57.89 (24.49)
8	S_0	−37.78 (−13.33)
9	S_0	−29.21 (−25.48)
CI-7	S_1/S_0	113.0 (110.1)
10	S_0	−78.37(−78.07)
11	S_0	−154.3 (−153.8)

[a] Energies were calculated at the MP2-CAS(6,6)/6-311G(d,p)//CAS-(6,6)/6-311G(d) and CAS(6,6)/6-311G(d) (values in parentheses) levels of theory. See Figures 6–9. [b] Energy relative to vinylidenecyclobutane (**6**).

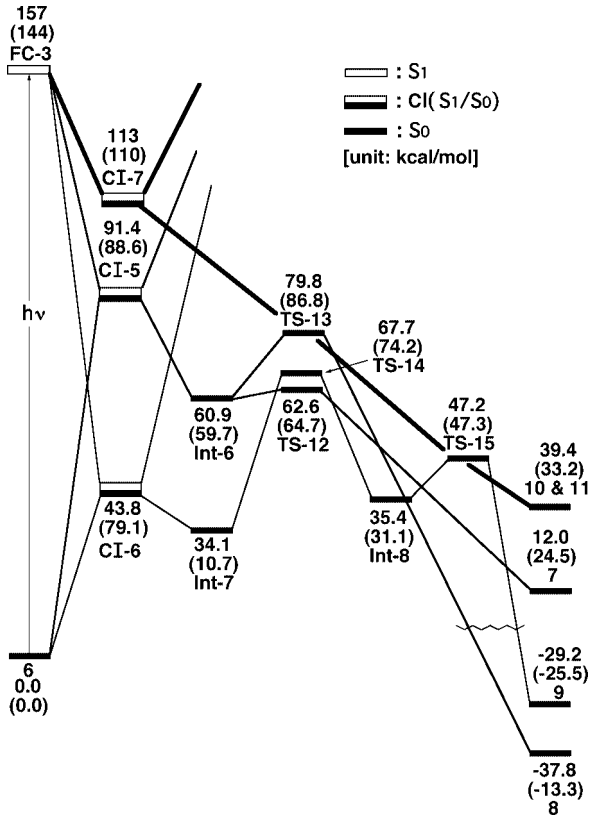

Figure 6. Energy profiles for the photoisomerization modes of vinylidenecyclobutane (**6**). FC, Franck−Condon; CI, conical intersection. Relative energies were obtained at the MP2-CAS-(6,6)/6-311G(d,p)// CAS(6,6)/6-311G(d) and CAS(6,6)/6-311G(d) (values in parentheses) levels of theory. All energies (in kilocalories per mole) are given with respect to the reactant (**6**). For CASSCF optimized structures of the crucial points, see Figures 7–9. For more information see the text.

and MP2-CAS calculations in Table 2. Cartesian coordinates and energetics calculated for the critical points at the CASSCF level are available as Supporting Information.

As in the case of spiro[2,4]hept-1-ene **1**, the singlet photorearrangement reactions of **2** studied in this work follow reaction paths similar to those shown earlier. On the basis of the CASSCF(6,6)/6-311G(d) structure of the ground state **2**, the vertical excitation energy from S_0 to S_1 [$S_0 \rightarrow S_1$ (S_0 geom)] was calculated to be about 152 kcal/mol (**FC-2**) above the ground-state reactant **2**. This value agrees well with the experimental value of 185 nm (= 155 kcal/mol in energy) obtained by irradiating a dilute solution of **6**.

Once the $S_0 \rightarrow S_1$ vertical excitation occurs, the system will relax from the **FC-2** point to the conical intersection points (**CI-3** and **CI-4**). Our MP2-CAS results suggest that **CI-3** and **CI-4** are 58 and 49 kcal/mol lower in energy than **FC-2**, respectively. The optimized geometrical parameters of **CI-3** and **CI-4** can be found in Figure 5. As mentioned earlier, both adopt vinylcarbene-like structures. In Figure 5, we also give the directions of the derivative coupling and gradient difference vectors for the **CI-3** and **CI-4** conical intersections. As a result, funneling through the **CI-3** and **CI-4** conical intersections may lead to two different reaction pathways on the ground-state surface via either the derivative coupling vector or the gradient difference vector direction.[7] On one hand, as can be seen in Figure 5 for **CI-3**, the major contribution of the gradient difference vector involves the alkylcyclopropene ring expansion, while the derivative coupling vector corresponds to a concerted CC bond stretching motion. Furthermore, following the gradient difference vector from **CI-3** leads to the formation of a vinylcarbene-like intermediate (**Int-3**) in the trans form. From this point, three reaction pathways (paths 7−9) were explored in this work. The search for transition states on the S_0 surface gives **TS-7**, **TS-8**, and **TS-9** for the products spiro[2,4]hept-1-ene **1** (path 7), alkyne **3** (path 8), and diene **4** (path 9), respectively. Their selected geometrical parameters are given in Figure C in Supporting Information. Additionally, our MP2-CAS computational results indicate that the energy of **TS-7**, **TS-8**, and **TS-9** relative to the vinylcarbene-like intermediate (**Int-3**) is 7.0, 14, and 21 kcal/mol, respectively. From the kinetic viewpoint, we thus predict that spiro[2,4]hept-1-ene (**1**) produced by path 7 should have the largest quantum yield of the three photoproducts.

Alternatively, we also located another vinylcarbene-like conical intersection, which was identified as **CI-4** in Figure 4. Its key structural parameters are given in Figure 5, accompanied by the derivative coupling vector and the gradient difference vector. These vectors correspond to changes in the C_1-C_3 and C_1-C_2 bond lengths, respectively. An increase in the C_1-C_3 bond length coupled with a decrease in the C_1-C_2 bond length leads to a local minimum, **Int-4**. It should be emphasized that this bending motion species (**CI-4**) is in accordance with the previous proposed vinylcarbene as mentioned in Scheme 2. Then, as one can see in Figure D in Supporting Information, from **Int-4** this intermediate undergoes C_2-C_7 bond formation to obtain **TS-10**. The theoretically calculated eigenvalue gives an imaginary frequency of 158*i* (**TS-10**) cm^{-1}. Indeed, inspection of the transition vector shows clearly that the reaction proceeds toward formation of a six-membered ring species (**Int-5**). Furthermore, the transition state located for the 1,2-H migration in path 10 is characterized by one imaginary frequency of 108*i* cm^{-1} for **TS-11**. The normal coordinate corresponding to the imaginary frequency is primarily located at the C−H bond cleavage. Again, from **TS-11** isomerization can take place in one direction, in which the 1,2-H shift occurs to form the final product **5**. As a result, the rearrangement reactions may be summarized as follows:

Path 7: **2** (S_0) + $h\nu \rightarrow$ **FC-2** $\rightarrow$ **CI-3** $\rightarrow$ **Int-3** $\rightarrow$ **TS-7** $\rightarrow$ **1**

Path 8: **2** (S_0) + $h\nu \rightarrow$ **FC-2** $\rightarrow$ **CI-3** $\rightarrow$ **Int-3** $\rightarrow$ **TS-8** $\rightarrow$ **3**

Path 9: **2** (S_0) + $h\nu$ → **FC-2** → **CI-3** → **Int-3** → **TS-9** → **4**

Path 10: **2** (S_0) + $h\nu$ →

FC-2 → **CI-4** → **Int-4** → **TS-10** → **Int-5** → **TS-11** → **5**

As discussed previously, path 7 has the lowest barrier height among paths 7−9. On the other hand, path 10 (**Int-4** → **TS-10**) possesses a barrier height computed to be about 58 kcal/mol. Due to the large excess energy of 122 kcal/mol obtained from the decay of **FC-2** to **Int-4**, this barrier can easily be surmounted. However, one can readily see that path 7 should be favored over path 10 from an energetic viewpoint. Besides this, path 7 is a four-step process, while path 10 is a six-step process. As a result, it presumably takes a longer time for the photorearrangement of **2** to occur via path 10, since it involves more steps to obtain the final photoproduct. Supporting experimental evidence comes from the fact that irradiation of **2** produces the products **1** (path 7), **3** (path 8), **4** (path 9), and **5** (path 10) in yields of 32%, 18%, 4.8%, and 4.9%, respectively.[2]

(3) Vinylidenecyclobutane (6). We have also investigated the photoisomerizations of vinylidenecyclobutane **6** (eq 3 in Scheme 1). The potential energy profiles for photoisomerization of **6** to produce various photoproducts at the MP2-CAS and CASSCF levels are given in Figure 6. Their selected geometrical parameters are collected in Figures 7–9, together with the nonadiabatic coupling and gradient difference vectors of the conical intersection points. The energies relative to the reactant molecule (**1**) are also listed in Table 3. Cartesian coordinates and energies calculated for the crucial points at the CASSCF level are available as Supporting Information.

The quality of the vinylidenecyclobutane **6** model has been tested by computing the S_1-S_0 energy gap at the Franck−Condon structure (see **FC-3** in Figure 6). Remarkably, the computed vertical excitation energy (157 kcal/mol) to the lowest excited π^* state of **6** is in good agreement with the experimental absorption of 185 nm (=155 kcal/mol) light by **6**.

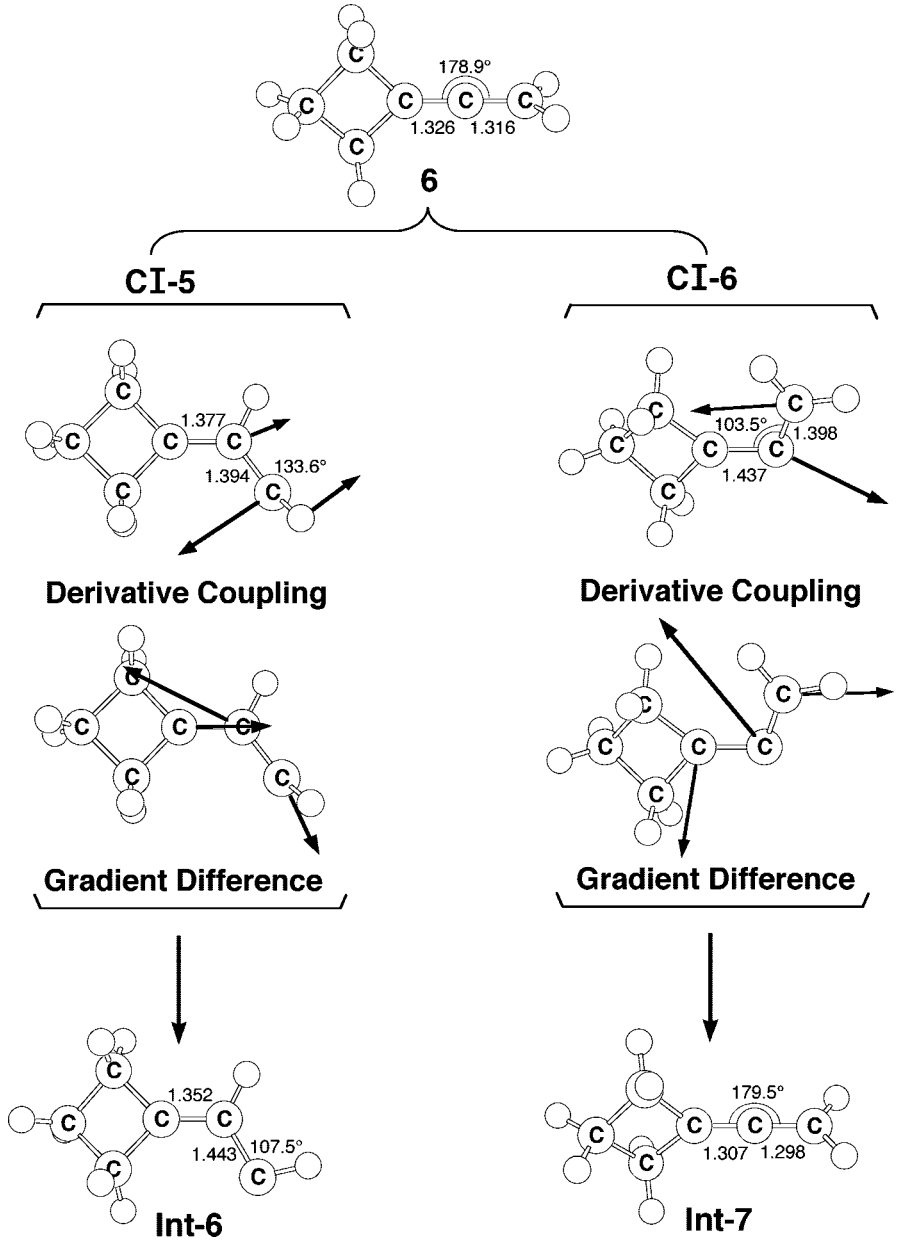

Figure 7. CAS(6,6)/6-311G(d,p) geometries (bond lengths in angstroms, angles in degrees) for paths 11−14 of vinylidenecyclobutane (**6**), conical intersections (**CI**), and intermediates (**Int**). Derivative coupling and gradient difference vectors—those that lift the degeneracy—were computed with CASSCF at **CI-5** and **CI-6**. Corresponding CASSCF vectors are shown as insets. Heavy arrows indicate the main atomic motions in the transition-state eigenvector. For more information see Supporting Information.

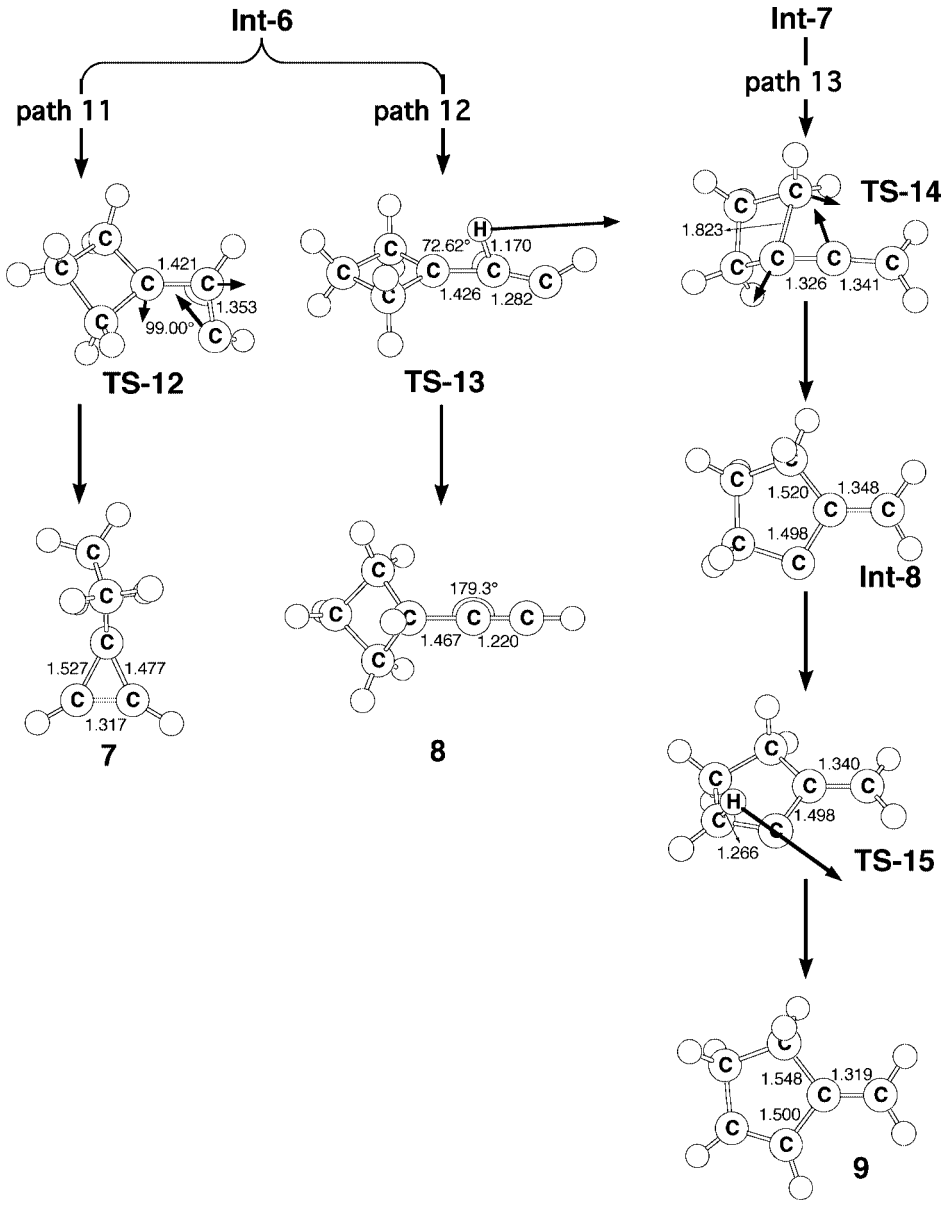

Figure 8. CAS(6,6)/6-311G(d) geometries (bond lengths in angstroms, angles in degrees) for paths 11−13 of vinylidenecyclobutane (**6**), transition states (**TS**), intermediates (**Int**), and isomer products. Heavy arrows indicate the main atomic motions in the transition-state eigenvector. Corresponding CASSCF vectors are shown as insets. For more information see Supporting Information.

We next investigated the subsequent process, relaxation on an excited-state potential surface. We searched for conical crossing points between the S_0 and S_1 surfaces for the three reaction pathways as given in eq 3 in Scheme 1. Specifically, the photochemically active relaxation path, starting from the S_1 excited state of **6**, leads to S_1/S_0 **CI-5** (paths 11 and 12), **CI-6** (path 13), and **CI-7** (path 14), which are shown in Figure 6.

The geometry at the conical intersection **CI-5** of C_1 symmetry is shown in Figure 7. As expected, **CI-5** adopts a vinylcarbene-like geometry. Our theoretical findings suggest that **CI-5** is 66 kcal/mol lower in energy than **FC-3** at the MP2-CAS level of theory. In Figure 7, we also give the directions of the derivative coupling and gradient difference vectors for **CI-5**. These vectors give an indication of the possible reaction pathways available on the ground-state surface after decay. As demonstrated in Figure 7, the major contribution of the gradient difference vector involves a three-membered ring opening, while the derivative coupling vector corresponds to a concerted CCH bending motion. Furthermore, following the gradient difference vector from **CI-5** leads to either the formation of a vinylcarbene-like species **Int-6** or a back reaction to the reactant **6**. From **Int-6**, the system undergoes either a C−C bond closing via transition state **TS-12** (path 11) or the 1,2-sigmatropic shift of the CH group via transition state **TS-13** (path 12) to give spiro[2,3]hex-1-ene (**7**) and ethynylcyclobutane (**8**), respectively. The geometry at the conical intersection **CI-6** (path 13) is also given in Figure 7. Again, from **CI-6** the isomerization can take place in one direction to yield the intermediate **Int-7**. Then, from **Int-7** the C_3-C_6 bond is broken and a C_2-C_6 bond is formed to form a five-membered ring species, the observed photoproduct **9**. As a result, our theoretical investigations suggest that the reaction mechanism of paths 11−13 should proceed as follows:

Path 11: **6** $(S_0) + h\nu \rightarrow$

FC-3 → **CI-5** → **Int-6** → **TS-12** → **7**

Path 12: **6** $(S_0) + h\nu \rightarrow$

FC-3 → **CI-5** → **Int-6** → **TS-13** → **8**

Path 13: **2** (S_0) + $h\nu$ →

FC-3 → CI-6 → Int-7 → TS-14 → Int-8 → TS-15 → 9

Our MP2-CAS computations shown in Table 3 and Figure 6 point out that the barrier heights from **Int-6** to **TS-12** (path 11), from **Int-6** to **TS-13** (path 12), and from **Int-6** to **TS-14** (path 13) are 1.7, 19, and 34 kcal/mol, respectively. Because of a large excess energy (96 and 123 kcal/mol) obtained from the decay of **FC-3** to **Int-6** and of **FC-3** to **Int-7**, these barriers can readily be surmounted. Our model calculations thus predict that path 11 should be much more favorable than paths 12 and 13 from the kinetic viewpoint. Indeed, it was reported that photolysis of **6** gives **7** (18%), **8** (14%), and **9** (23%).[5] Accordingly, our theoretical predictions presented in this work are in qualitative agreement with the experimental observations.[5]

On the other hand, we also explored the mechanism of path 14, which contains only one conical intersection point (**CI-7**). The derivative coupling and gradient difference vectors obtained at the conical intersection are given in Figure 9. As seen in Figure 6, the MP2-CAS results suggest that **CI-7** is lower in energy than **FC-3** by 42 kcal/mol but higher in energy than its corresponding reactant **6** by 115 kcal/mol. Comparing this to the previous reaction pathways (paths 11−13), one may easily see that path 14 is the least favorable of these four reaction pathways from an energetic viewpoint. In particular, as one can see in Figure 9, the derivative coupling vector of **6** in **CI-7** can lead to two C−C bonds breaking, which can form ethylene (**10**) and a linear molecule (**11**). As a result, our computational results suggest that the mechanism for path 14 should be represented as follows:

Path 14: **6** (S_0) + $h\nu$ → **FC-3** → **CI-7** → **10**,**11**

V. Conclusion

The photochemical mechanisms (Scheme 1) of spiro[2,4]hept-1-ene **1** (eq 1), 1-vinylcyclopentene **4** (eq 2), and vinylidenecyclobutane **6** (eq 3) have been investigated in this work. Taking all these systems studied in this paper together, one can obtain following conclusions:

SCHEME 3

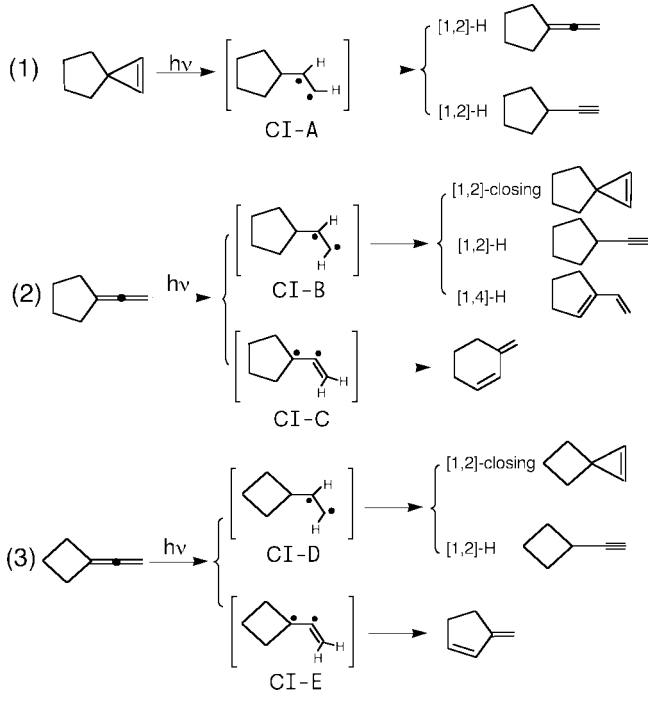

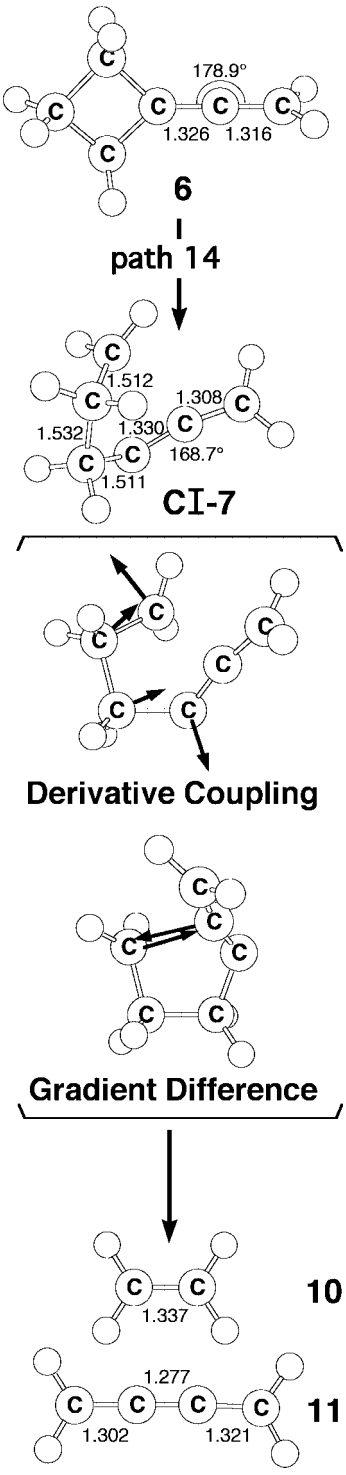

Figure 9. CAS(6,6)/6-311G(d) geometries (bond lengths in angstroms, angles in degrees) for path 14 of vinylidenecyclobutane (**6**), conical intersection (**CI**), and isomer products. Heavy arrows indicate the main atomic motions in the transition-state eigenvector. For more information see Supporting Information.

We can elaborate on the standard model of the photochemistry of spirocyclopropene derivatives. Scheme 3 summarizes the results of our theoretical and experimental investigations of the photochemistry of cyclopropene derivatives described above, showing the role of vinylcarbene-like intermediates. That is, photolysis of these compounds (**1**, **4**, and **6**) yields a variety of products, most of which are formally derived from the vinylcarbene-like species formed by either cleavage of one C−C σ bond or by a 1,2-hydrogen shift in the excited singlet state. The

vinylcarbene-like species, which can serve as a funnel in the conical intersection, are formed in the S_1 state from the S_0 cyclopropene derivative. Indeed, our theoretical investigations indicate that the structures of these funnels are vinylcarbene-like. Then, the molecule can decay to products by ring closure or hydrogen migration after internal conversion to the S_0 surface. Knowledge of the conical intersections of cyclopropene derivatives is of great importance in understanding their reaction mechanisms since it can affect the driving force for photochemistry. That is, the conical intersections can efficiently funnel molecules from the $^1(\pi\pi^*)$ state to the ground-state surface. As a result, these funnels, which are easily accessed once the $^1(\pi\pi^*)$ surface is populated, determine the reaction path taken on the ground-state surface.[7] Consequently, these findings, based on the conical intersection viewpoint, have helped us to better understand the photochemical reactions and to support the experimental observations.[2–5]

Acknowledgment. I am grateful to the National Center for High-Performance Computing of Taiwan for generous amounts of computing time and to the National Science Council of Taiwan for the financial support. I also thank Professor Michael A. Robb and Dr. Michael J. Bearpark, (University of London) and Professor Massimo Olivucci (Universita degli Studi di Siena) for their encouragement and support. Special thanks are also due to the reviewers for very helpful suggestions and comments.

Supporting Information Available: Additional geometric information. This material is available free of charge via the Internet at http://pubs.acs.org.

References and Notes

(1) For reviews, see (a) Padwa, A. *Org. Photochem.* **1979**, *4*, 261. (b) Padwa, A. *Acc. Chem. Res.* **1979**, *12*, 310. (c) Steinmetz, M. G.; Srinivasan, R.; Leigh, W. J. *Rev. Chem. Intermed.* **1984**, *5*, 57, and references cited therein.

(2) Leigh, W. J. *Chem. Rev.* **1993**, *93*, 487.

(3) Steinmetz, M. G.; Yen, Y.-P.; Poch, G. K. *J. Chem. Soc., Chem. Commun.* **1983**, 1504.

(4) Fahie, B. J.; Leigh, W. J. *Can. J. Chem.* **1989**, *67*, 1859, and references cited therein.

(5) Steinmetz, M. G.; Stark, E. J.; Yen, Y.-P.; Mayes, R. T.; Srinivasan, R. *J. Am. Chem. Soc.* **1983**, *105*, 7209.

(6) For instance, see (a) Greenberg, A.; Liebman, J. F. *Strained Organic Molecules*; Academic Press: New York, 1978. (b) Kobrich, G. *Angew. Chem., Int. Ed. Engl.* **1973**, *12*, 464. (c) De Mayo, P. In *Rearrangements in Ground and Excited States*; Academic Press: New York, 1980; Vol. 3, p501. (d) Salaun, J. *Top. Curr. Chem.* **2000**, *207*, 1. (e) Gnad, F.; Reiser, O. *Chem. Rev.* **2003**, *103*, 1603. (f) Rubina, M.; Rubin, M.; Gevorgyan, V. *J. Am. Chem. Soc.* **2004**, *126*, 3688. (g) Liao, L.; Zhang, F.; Dmitrenko, O.; Bach, R. D.; Fox, J. M. *J. Am. Chem. Soc.* **2004**, *126*, 4490. (h) Chuprkov, S.; Rubin, M.; Gevorgyan, V. *J. Am. Chem. Soc.* **2005**, *127*, 3714. (i) Nowlan, D. T., III; Singleton, D. A. *J. Am. Chem. Soc.* **2005**, *127*, 6190. (j) Liu, X.; Fox, J. M. *J. Am. Chem. Soc.* **2006**, *128*, 5600. (k) Oulie, P.; Boulho, C.; Vendier, L.; Coppel, Y.; Etienne, M. *J. Am. Chem. Soc.* **2006**, *128*, 15962.

(7) (a) Bernardi, F.; Olivucci, M.; Robb, M. A. *Isr. J. Chem.* **1993**, 265. (b) Klessinger, M. *Angew. Chem., Int. Ed. Engl.* **1995**, *34*, 549. (c) Bernardi, F.; Olivucci, M.; Robb, M. A. *Chem. Soc. Rev.* **1996**, 321. (d) Bernardi, F.; Olivucci, M.; Robb, M. A. *J. Photochem. Photobiol. A: Chem.* **1997**, *105*, 365. (e) Klessinger, M. *Pure Appl. Chem.* **1997**, *69*, 773.

(8) Frisch, M. J.; Trucks, G. W.; Schlegel, H. B.; Scuseria, G. E.; Robb, M. A.; Cheeseman, J. R.; Zakrzewski, V. G.; Montgomery, Jr., J. A.; Stratmann, R. E.; Burant, J. C.; Dapprich, S.; Millam, J. M.; Daniels, A. D.; Kudin, K. N.; Strain, M. C.; Farkas, O.; Tomasi, J.; Barone, V.; Cossi, M.; Cammi, R.; Mennucci, B.; Pomelli, C.; Adamo, C.; Clifford, S.; Ochterski, J.; Petersson, G. A.; Ayala, P. Y.; Cui, Q.; Morokuma, K.; Malick, D. K.; Rabuck, A. D.; Raghavachari, K.; Foresman, J. B.; Cioslowski, J.; Ortiz, J. V.; Baboul, A. G.; Stefanov, B. B.; Liu, Liashenko, G.; Piskorz, A.; Komaromi, P. I.; Gomperts, R.; Martin, R. L.; Fox, D. J.; Keith, T.; Al-Laham, M. A.; Peng, C. Y.; Nanayakkara, A.; Gonzalez, C.; Challacombe, M.; Gill, P. M. W.; Johnson, B.; Chen, W.; Wong, M. W.; Andres, J. L.; Gonzalez, C.; Head-Gordon, M.; Replogle, E. S.; Pople, J. A. *Gaussian 03*; Gaussian, Inc.: Pittsburgh, PA, 2003.

(9) Hehre, W. J.; Radom, L.; Schleyer, P. v. R.; Pople, J. A. *Ab Initio Molecular Orbital Theory*; Wiley: New York, 1986.

(10) Bearpark, M. J.; Robb, M. A.; Schlegel, H. B. *Chem. Phys. Lett.* **1994**, *223*, 269.

(11) Fukui, K. *J. Phys. Chem.* **1970**, *74*, 4161.

(12) Gonzalez, C.; Schlegel, H. B. *J. Phys. Chem.* **1989**, *90*, 2154.

(13) McDouall, J. J. W.; Peasley, K.; Robb, M. A. *Chem. Phys. Lett.* **1988**, *148*, 183.

JP711022N